

Maximum Power Point Tracking of Photovoltaic Systems Based on Fast Terminal Sliding Mode Controller

A.Zaidi*[‡], K.Dahech*, T.Damak*

*Laboratory of Sciences and Techniques of Automatic Control and Computer Engineering (Lab-STA), National School of Engineering of Sfax (ENIS), University of Sfax. Postal Box 1173, 3038 Sfax, Tunisia

(zaidi.asma85@gmail.com, dahechkarim@yahoo.fr, tarak.damak@enis.rnu.tn)

[‡]Corresponding Author: A.Zaidi; zaidi.asma85@gmail.com

Received: 29.06.2016 Accepted: 22.09.2016

Abstract- This work introduces a maximum power point tracking method based on fast terminal sliding mode control (FTSMC) for photovoltaic systems. The control scheme contains two loops: the first achieves the maximum power point (MPP) searching via an algorithm which gives the reference voltage (MPV). The second loop achieves regulation of the operating point to the reference MPV issued from the first loop. Unlike the traditional sliding mode, the FTSM controller guarantees finite time convergence of the MPPT with robustness. Control performances are proved through several simulations.

Keywords: Fast Terminal sliding mode control (FTSMC); Maximum power point tracking (MPPT), PV module.

1. Introduction

The increasing concern about the growing energy consumption, global warming and the diminishing of fossil fuels have made renewable energy more and more popular. Renewable energy has diverse forms such as: wind, geothermic, photovoltaic and hydraulic energies. The photovoltaic energy is one of the most efficient alternative resources due to its different benefits. In fact, the PV energy is environment friendly and has lower cost of fixing. Meanwhile, PV modules should be gathered in series and parallel to attain high levels of solar energy. Nevertheless, they are sometimes subject to shading conditions such as: dust, surrounding buildings, clouds and trees. Therefore, the shaded PV module is no more competent and it is assimilated to a load. This could damage PV module cells. The challenge is to maximize PV system efficiency even when the PV module is exposed to non-uniform radiations. In literature, there are diverse types of algorithms which drive the PV module to the peak of the solar power generation, this is called MPPT: Maximum power point tracking. P&O method [1,2,3], incremental conductance [4,5], artificial neural networks [6,7] and fuzzy logic [8,9] are the most commonly

found techniques in literature. Unfortunately, these algorithms provide only near maximum power and don't offer an accurate convergence when PV module is subject to non-uniform insolation conditions. So in order to resolve this dilemma, other MPPT techniques are designed by using two-loop control [10,11]. This allows easy implementation and ensures stability of the whole PV generation system. In fact, the first loop provides the maximum power voltage (MPV), and the other loop ensures regulation of the MPV. The impedance adjustment between PV module and load is conducted through a DC/DC converter which operates at the corresponding MPP. As the tracking performance is strongly related to the second loop, the parameter uncertainties and disturbances will influence the control behavior. Therefore, most of the two-loop control approaches are subject to chattering around the desired operating point MPP. In order to avoid these drawbacks, sliding mode control (SMC) [12,13,14] is utilized owing to its powerful ability to control system having uncertainties.

Terminal SMC (TSMC) is one of the most used schemes of SMC that can fulfill finite-time stability [15,16] and shows robust behavior against uncertainties and external perturbations.

By using nonlinear sliding mode, TSMC provides a finite-time error convergence. Owing to this idea, many researches have been developed to design TSMC methods with high-order systems [17], MIMO linear systems [18] and uncertain dynamic systems [19]. Meanwhile, when the states are distant from the equilibrium, TSMC cannot offer the same convergence performances. To defeat this difficulty, Yu and Man [20] presented the fast TSMC (FTSMC) method that can fulfill fast finite-time convergence when states are close or distant from the equilibrium. Nevertheless, singularity problems are met in both TSMC and FTSMC, and this subject was treated succinctly in literature [21,22].

In this work, a FTSM controller for photovoltaic systems is designed. Voltage reference is given from the MPP searching algorithm in the first loop. In the second loop, the FTSM controller is used to move the operating point to the reference voltage. Furthermore, FTSMC provides convergence in limited time and then the MPV is precisely reached. Meanwhile, the proposed FTSMC is robust against disturbances and uncertainties. The designed method offers high performances compared with conventional MPPT techniques due to the reduction of power oscillation.

The paper is divided as follows: the mathematical model of the used PV structure is addressed in Section 2. The structure of the MPPT based on a FTSMC is described in section 3.1 and 3.2. Next, the robustness analysis issue of the designed control scheme is given in section 3.3. Section 4 describes two conventional searching algorithms in order to compare them with the proposed controller. Section 5 illustrates simulation results for constant and varying radiation. Section 6 contains conclusions issued from this work.

2. Mathematical Modelling of the Photovoltaic Power Generation System

The power generation system contains a photovoltaic module gathered with a boost converter used to adjust output voltage V_{pv} and consequently obtain a maximum solar power generation. The scheme of the used PV structure is presented in Fig.1.

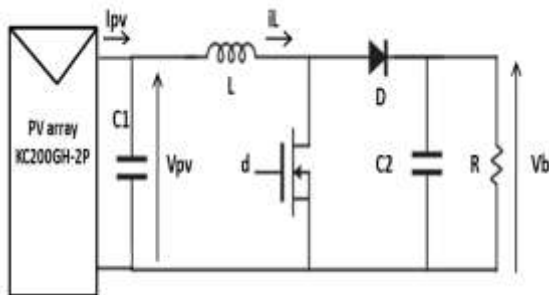


Fig.1. Scheme of the used PV structure.

The PV generator has n_s cells connected in series and n_p panels parallelly connected. Basic model of an elementary cell is given in Fig.2.

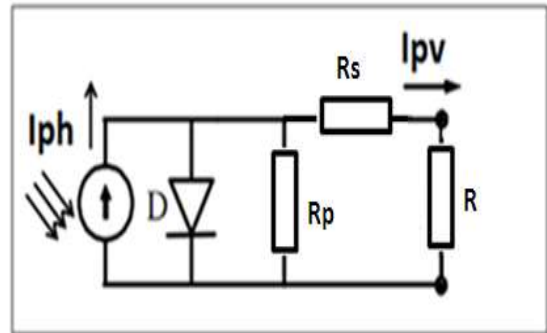


Fig.2. A basic model of an elementary cell.

The considered system is described by the equation below [23].

$$I_{pv} = n_p I_{ph} - n_p I_{sat} \left[\exp \left(\frac{q}{nk_b T} \left(\frac{V_{pv} + I_{pv} R_s}{n_s} \right) \right) - 1 \right] - \frac{V_{pv} + I_{pv} R_s}{R_p} \quad (1)$$

In equation (1), the used symbols are specified as: I_{pv} is the current of the photovoltaic module (A); V_{pv} is the voltage of the photovoltaic module (V); I_{ph} is the light-generated current (A); I_{sat} is the inverse saturation current, (A); R_s is the PV cell series resistance, (Ω); R_p is the PV cell parallel resistance (Ω); n is the ideality factor; q is the charge of electron; k_b is the constant of Boltzmann; T is the temperature of the photovoltaic cell; However, R_s is very tiny and R_p is much greater than R_s so both could be ignored and equation (1) can be reduced as follows.

$$I_{pv} = n_p I_{ph} - n_p I_{sat} \left[\exp \left(\frac{q}{nk_b T} \frac{V_{pv}}{n_s} \right) - 1 \right] \quad (2)$$

Furthermore, the value of I_{sat} is strongly influenced by the PV cell temperature, this relation is described in the following equation:

$$I_{sat} = I_0 \left(\frac{T}{T_0} \right)^{\frac{3}{n}} \exp \left[\frac{q E_{gap}}{nK} \left(\frac{1}{T_0} - \frac{1}{T} \right) \right] \quad (3)$$

Where T_0 is the ambient temperature, I_0 is the inverse saturation current at T_0 , E_{gap} is the band-gap energy. Nevertheless, the radiation E and the temperature T impact powerfully I_{ph} , this dependence is described in the equation below:

$$I_{ph} = I_{sc0} E + K_l (T - T_0) \quad (4)$$

Where I_{sc0} is the short circuit current of the photovoltaic module at T_0 and K_l is the short-circuit current temperature coefficient.

Considering equation (2), the power of the photovoltaic module is expressed as

$$P_{pv} = V_{pv} I_{pv} \quad (5)$$

$$P_{pv} = n_p I_{ph} V_{pv} - n_p I_{sat} V_{pv} \left[\exp\left(\frac{q}{nk_b T} \frac{V_{pv}}{n_s}\right) - 1 \right] \quad (6)$$

This equation shows obviously that the power generation of the PV module depends on temperature and insolation levels. In order to investigate the effect of these two climatic factors, the PV module curve ($P_{pv} - V_{pv}$) is plotted. The simulation conducted under various solar irradiance levels and a 25°C temperature is shown in Fig.3. The same simulation for a fixed value of radiation $E = 1000W/m^2$ and various temperatures is given in Fig.4.

It's obvious that the maximum power varies when radiation and temperature vary too. In fact, when insolation levels rise, the power and the output current increase. Meanwhile, boosting temperature induce the diminishing of the open circuit voltage values. Besides, characteristic curve exhibits a unique V_{pv} in which the maximum power is attained.

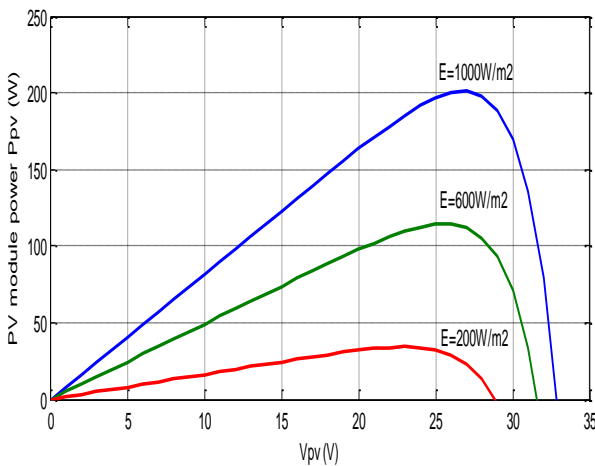


Fig.3. $P_{pv} - V_{pv}$ characteristic under varying solar radiations

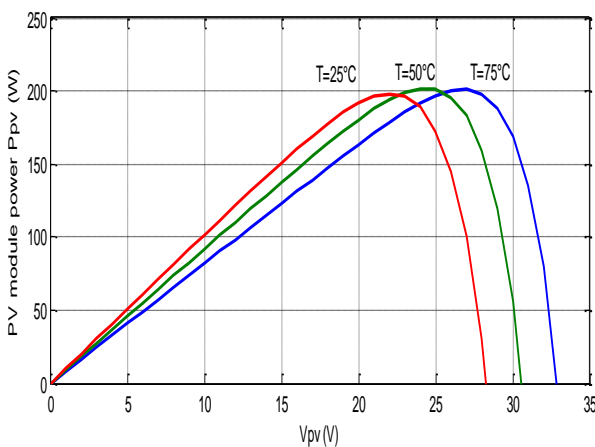


Fig.4. $P_{pv} - V_{pv}$ characteristic under varying temperatures

Absorbing maximum solar power requires a boost converter between PV module and load. Utilizing time average method [24] leads to the following mathematical

structure of the boost converter. This model is described by the equations below:

$$\begin{aligned} \frac{dV_{pv}}{dt} &= -\frac{1}{C_1}(i_L - I_{pv}) \\ \frac{di_L}{dt} &= \frac{1}{L}V_{pv} - \frac{R_c(1-d)}{L(1+\frac{R_c}{R})}i_L + \frac{1-d}{L}\left(\frac{R_c}{R+R_c} - 1\right)V_b \\ &\quad - V_D \frac{(1-d)}{L} \\ \frac{dV_b}{dt} &= \frac{(1-d)L}{C_2(1+\frac{R_c}{R})}i_L - \frac{1}{C_2(R+R_c)}V_b \end{aligned} \quad (7)$$

Where d is the switch duty ratio, V_{pv}, V_b and i_L are respectively the voltage issued from the photovoltaic module, the voltage issued from the boost converter and the inductor current; R_c is capacitance C_2 internal resistance, R is the load resistance; V_D is the forward voltage of the diode. Adjusting the PWM duty cycle d in order to make V_{pv} coincide with the MPP even when the climate conditions change is the aim of the control. To accomplish this, a FTSM-based controller is proposed.

3. MPPT Controller Based on Fast Terminal Sliding Mode

Figure 5 illustrates the bloc scheme used in order to obtain MPP under radiation and temperature variation. In this case, I_{pv} and V_{pv} are used as input for the MPPT searching algorithm. This first loop calculates the reference maximum power voltage V_{ref} . In the second loop, V_{ref} serves as an input for the Fast terminal sliding mode controller to achieve MPPT.

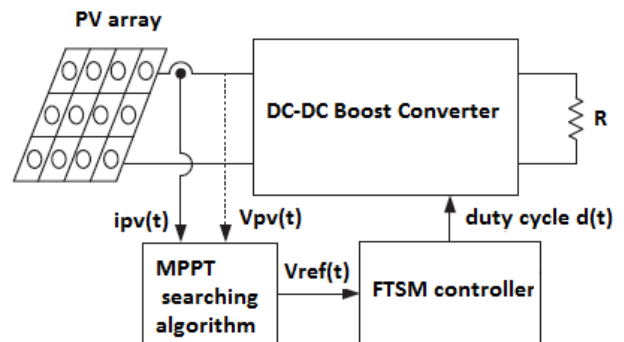


Fig.5. Proposed MPPT bloc scheme.

3.1. Determining maximum power point [25]

When the output voltage issued from the photovoltaic module reaches the MPP, the following equality is satisfied:

$$\frac{d}{dI_{pv}}(V_{pv}I_{pv}) = 0 \quad (8)$$

Consequently,

$$V_{pv} + I_{pv} \frac{dV_{pv}}{dI_{pv}} = 0 \tag{9}$$

When the maximum power is reached, $I_{pv} = I_{mpp}$. Replacing V_{pv} and dV_{pv}/dI_{pv} by their expressions in (8) yields:

$$\ln\left(\frac{I_{ph} - I_{mpp} + I_{sat}}{I_{ph}}\right) - \frac{I_{mpp}}{I_{ph} - I_{mpp} + I_{sat}} = 0 \tag{10}$$

Solving (10) leads to the following linear equation relying I_{mpp} and I_{ph} :

$$I_{mpp} = 0.909 I_{ph} \tag{11}$$

From I_{ph} and I_{pv} , V_{ref} and V_{pv} are determined as follows:

$$V_{ref} = 0.909 I_{ph} \tag{12}$$

3.2. FTSM-based controller

3.2.1. Problem formulation

The controller aim is to adjust duty cycle d . First, let $x_1(t) = V_{pv}(t)$, $x_2(t) = i_L(t)$, $x_3(t) = V_b(t)$, $x_{1ref}(t) = V_{ref}(t)$ and the structure (7) becomes:

$$\begin{aligned} \dot{x}_1 &= \frac{-x_2 + I_{pv}}{C_1} \\ \dot{x}_2 &= f_1(x) + g_1(x)d(t) \end{aligned} \tag{13}$$

$$\dot{x}_3 = f_2(x) + g_2(x)d(t)$$

Where $x = [x_1 \ x_2 \ x_3]^T$;

$$f_1(x) = \frac{x_1}{L} - \frac{R_C}{L(1 + \frac{R_C}{R})}x_2 + \frac{1}{L}\left(\frac{R_C}{R + R_C} - 1\right)x_3 - \frac{V_D}{L} \tag{14}$$

$$g_1(x) = -\frac{R_C}{L(1 + \frac{R_C}{R})}x_2 - \frac{1}{L}\left(\frac{R_C}{R + R_C} - 1\right)x_3 + \frac{V_D}{L} \tag{15}$$

$$f_2(x) = \frac{1}{C_2(1 + \frac{R_C}{R})}x_2 - \frac{1}{C_2(R + R_C)}x_3 \tag{16}$$

$$g_2(x) = -\frac{1}{C_2(R + \frac{R_C}{R})}x_2 \tag{17}$$

The designed controller is used to allow V_{pv} reach the MPP reference voltage V_{ref} . When V_{pv} attains V_{ref} , the entire PV system will operate at the peak of the $(P_{pv} - V_{pv})$ curve during the MPP searching algorithm adjustment.

As a first step, let us introduce the voltage tracking error:

$$e_1 = x_1 - x_{1ref} \tag{18}$$

Differentiating e_1 with respect to time yields,

$$\dot{e}_1 = \frac{1}{C_1}(I_{pv} - x_2) - \dot{x}_{1ref} \tag{19}$$

We introduce a novel tracking error

$$e_2 = x_2 - x_{2ref} \text{ where } x_{2ref} = I_{pv} - C_1 \dot{x}_{1ref}.$$

Then, we obtain the new derivatives of the two tracking errors as follow:

$$\dot{e}_1 = -\frac{e_2}{C_1} \tag{20}$$

$$\dot{e}_2 = f_1(x) - \dot{x}_{2ref} + g_1(x)d(t) \tag{21}$$

$$\text{Where } \dot{x}_{2ref} = \frac{dI_{pv}}{dt} - C_1 \frac{d^2 x_{1ref}}{dt^2}.$$

Let $z_1 = e_1$ and $z_2 = -\frac{e_2}{C_1}$ and the system equations (20)

and (21) are rewritten as follows:

$$\begin{aligned} \dot{z}_1 &= z_2 \\ \dot{z}_2 &= f_3(x) + g_3(x)d(t) \end{aligned} \tag{22}$$

Where $f_3(x) = -\frac{1}{C_1}(f_1(x) - \dot{x}_{2ref})$ and $g_3(x) = -\frac{g_1(x)}{C_1}$

The system (22) is a degree 2 non-linear single-input-single-output (SISO) system. Now in order to design the control law $d(t)$ and consequently allow z_1 and z_2 reach equilibrium point in limited time, we choose the following recursive structure of FTSM [26] expressed as follows:

$$\begin{aligned} s_1 &= \dot{s}_0 + \alpha_0 s_0 + \beta_0 s_0^{p_0/q_0} \\ s_2 &= \dot{s}_1 + \alpha_1 s_1 + \beta_1 s_1^{p_1/q_1} \\ &\dots \end{aligned} \tag{23}$$

$$\begin{aligned} s_{n-1} &= \dot{s}_{n-2} + \alpha_{n-2} s_{n-2} + \beta_{n-2} s_{n-2}^{p_{n-2}/q_{n-2}} \\ s_0 &= z_1 \end{aligned}$$

Where $\alpha_i, \beta_i > 0$; $p_i, q_i (p_i < q_i) (i = 0, 1, \dots, n-2)$; $p_i > 0$; $q_i > 0$.

In fact, this structure allows us to avoid using the conventional control design principle :

$s_{n-1} \dot{s}_{n-1} < -k |s_{n-1}|$ which causes the chattering phenomenon.

3.2.2. Stability Analysis

In this paper, we choose the following recursive sliding surfaces:

$$s_0 = z_1$$

$$s_1 = \dot{s}_0 + \alpha_0 s_0 + \beta_0 s_0^{\frac{p_0}{q_0}} \tag{24}$$

Theorem 1:

Considering system (22), if the control law $d(t)$ is chosen as follows:

$$d(t) = -\frac{1}{g_3(x)} [f_3(x) + \alpha_0 \dot{s}_0 + \beta_0 \frac{p_0}{q_0} \dot{s}_0 s_0^{\frac{p_0}{q_0}-1} + \alpha_1 s_1 + \beta_1 s_1^{\frac{p_1}{q_1}}] \tag{25}$$

Where $\alpha_1, \beta_1 > 0, 0 < \frac{p_1}{q_1} < 1$, and $g_3(x) \neq 0$ for all $x(t)$.

The states will attain $s_1 = 0$ in limited time t_{s_1} given by the following expression:

$$t_{s_1} = \frac{q_1}{\alpha_1(q_1 - p_1)} \text{Ln}\left(\frac{\alpha_1 z_1(0)^{\frac{(q_1-p_1)}{q_1}} + \beta_1}{\beta_1}\right) \tag{26}$$

Proof

To demonstrate the previous theorem, the following Lemma is introduced.

Lemma1[27]

Admit that a continuous positive-definite function $\Gamma(t)$ fullfills the following differential inequality:

$$\dot{\Gamma}(t) \leq -a\Gamma^\mu ; \forall t \geq t_0, \Gamma(t_0) \geq 0$$

Where $a > 0, 0 < \mu < 1$ are constants.

Then $\Gamma(t) = 0, \forall t \geq t_1$ where t_1 is given by the following expression:

$$t_1 = t_0 + \frac{\Gamma^{1-\mu}(t_0)}{a(1-\mu)}$$

Deriving s_1 with respect to time yields:

$$\begin{aligned} \dot{s}_1 &= \dot{s}_0 + \alpha_0 \dot{s}_0 + \beta_0 \frac{p_0}{q_0} \dot{s}_0 s_0^{\frac{p_0}{q_0}-1} \\ &= f_3(x) + g_3(x)d(t) + \alpha_0 \dot{s}_0 + \beta_0 \frac{p_0}{q_0} \dot{s}_0 s_0^{\frac{p_0}{q_0}-1} \end{aligned} \tag{27}$$

Substituting the control law (25) into (27), the derivative of s_1 becomes:

$$\dot{s}_1 = -\alpha_1 s_1 - \beta_1 s_1^{\frac{p_1}{q_1}} \tag{28}$$

Now, we consider the Lyapunov candidate function V given by the following expression:

$$V = \frac{1}{2} s_1^2 \tag{29}$$

Taking the derivative of V , we can get:

$$\begin{aligned} \dot{V} &= s_1 \dot{s}_1 \\ &= s_1 \left(-\alpha_1 s_1 - \beta_1 s_1^{\frac{p_1}{q_1}} \right) \\ &= -\alpha_1 s_1^2 - \beta_1 s_1^{\frac{p_1}{q_1}+1} \\ &\leq -\beta_1 2^{\frac{p_1+q_1}{2q_1}} V^{\frac{p_1+q_1}{2q_1}} \end{aligned} \tag{30}$$

So, the system will attain $s_1 = 0$ in limited time according to Lemma 1. Consequently, the states z_1 and z_2 will reach zero and therefore e_1 and e_2 will move to zero in limited time t_{s_1} given by the resolution of the following equation:

$$s_1 + \alpha_1 s_1 + \beta_1 s_1^{\frac{p_1}{q_1}} = 0 \tag{31}$$

By rearranging equation (31), we obtain:

$$s_1^{\frac{p_1}{q_1}} \frac{ds_1}{dt} + \alpha_1 s_1^{1-\frac{p_1}{q_1}} = -\beta_1 \tag{32}$$

By making the following variable change $y = s_1^{1-\frac{p_1}{q_1}}$, equation (32) becomes:

$$\frac{dy}{dt} + \frac{q_1 - p_1}{q_1} \alpha_1 y = -\frac{q_1 - p_1}{q_1} \beta_1 \tag{33}$$

The first-order linear differential equation:

$$\frac{dy}{dx} + \Phi(x)y = \Psi(x)$$

has a general solution expressed as follows:

$$y = e^{-\int \Phi(x)dx} \left(\int \Psi(x) e^{\int \Phi(x)dx} dx + C \right)$$

Then the solution for the equation (33) is

$$y = e^{-\int_0^t \frac{q_1-p_1}{q_1} \alpha_1 d\tau} \left(\int_0^t -\frac{q_1-p_1}{q_1} \beta_1 e^{\int_0^{\tau} \frac{q_1-p_1}{q_1} \alpha_1 d\tau} d\tau + C \right) \tag{34}$$

When $t = 0, C = y(0)$, equation (34) is rewritten as follows:

$$y = -\frac{\beta_1}{\alpha_1} + \frac{\beta_1}{\alpha_1} e^{-\frac{(q_1-p_1)}{q_1} \alpha_1 t} + y(0) e^{-\frac{q_1-p_1}{q_1} \alpha_1 t} \tag{35}$$

When $s_1 = 0, y = 0$ and $t = t_s$, equation (35) becomes:

$$\frac{(\beta_1 + \alpha_1 y(0))}{\beta_1} = e^{-\frac{(q_1-p_1)}{q_1} \alpha_1 t_{s_1}}$$

Replacing $y(0)$ by its expression yields:

$$t_{s_1} = \frac{q_1}{\alpha_1(q_1 - p_1)} \text{Ln}\left(\frac{\alpha_1 z_1(0)^{\frac{(q_1-p_1)}{q_1}} + \beta_1}{\beta_1}\right) \tag{36}$$

And then the proof is completed.

3.3. Robustness analysis

Passive components induce parameter uncertainties responsible of the uncertain form of the considered boost converter. Moreover, the controlled system could be affected by external disturbances. Ameliorating its robustness requires the redesigning of parameters of the FTSM controller. First, assume that:

$$f_3 = \hat{f}_3(x) + \Delta f_3 \tag{37}$$

$$g_3 = \hat{g}_3(x) + \Delta g_3$$

Then, system (22) is rewritten as follows:

$$\begin{aligned} \dot{z}_1 &= z_2 \\ \dot{z}_2 &= \hat{f}_3(x) + \Delta f_3 + (\hat{g}_3(x) + \Delta g_3)d(t) \end{aligned} \tag{38}$$

Where \hat{f}_3, \hat{g}_3 are known and measurable, $\Delta f_3, \Delta g_3$ are the uncertain quantities generated by errors of measurements and system uncertainties. These uncertain parts are bounded as follow:

$$|\Delta f_3| < \xi; (\xi > 0) \tag{39}$$

$$|\Delta g_3| < \omega; (\omega > 0); \tag{40}$$

$$\frac{g_3}{\hat{g}_3} > 0; \tag{41}$$

Assume that:

$$\left| \Delta f_3 - b\hat{f}_3 - b(\alpha_0 s_0 + \beta_0 \frac{p_0}{q_0} s_0 s_0^{\frac{p_0-1}{q_0}}) \right| < L; \tag{42}$$

(L > 0)

Where $b = \frac{\Delta g_3}{\hat{g}_3}$

The proposed FTSMC fulfills MPPT and guarantees robustness to uncertainties at the same time according to theorem 2.

Theorem 2:

For system (38), if $d(t)$ is chosen as follows:

$$d(t) = -\frac{1}{\hat{g}_3} [\hat{f}_3 + \alpha_0 s_0 + \beta_0 \frac{p_0}{q_0} s_0 s_0^{\frac{p_0-1}{q_0}}] + \lambda s_1 + \mu s_1^{\frac{v}{w}} \tag{43}$$

Where $\lambda > 0; \mu > 0$ and $0 < \frac{v}{w} < 1$

So the states will attain the neighborhood Δ of the surface $s_1 = 0$ in finite time according to the attractor:

$$\dot{s}_1 = -\lambda_1 s_1 - \mu_1 s_1^{\frac{v}{w}} \tag{44}$$

Where

$$\lambda_1 = \lambda(b + 1) > 0 \tag{45}$$

$$\mu_1 = \mu(b + 1) - \frac{\Delta f_3 - b\hat{f}_3 - bA}{s_1^{\frac{v}{w}}} \tag{46}$$

$$\mu(b + 1) = \sigma + \frac{L}{|s_1|^{\frac{v}{w}}}; \sigma > 0;$$

$$\text{And } \Delta = \left\{ z: |s_1| > \left[\frac{L}{\mu(b+1)} \right]^{\frac{w}{v}} \right\} \tag{47}$$

Proof:

Taking into account uncertainties, the derivative of s_1 becomes:

$$\begin{aligned} \dot{s}_1 &= \hat{f}_3(x) + \Delta f_3 + (\hat{g}_3(x) + \Delta g_3)d(t) + \alpha_0 s_0 \\ &\quad + \beta_0 \frac{p_0}{q_0} s_0 s_0^{\frac{p_0-1}{q_0}} \end{aligned} \tag{48}$$

Let $A = \alpha_0 s_0 + \beta_0 \frac{p_0}{q_0} s_0 s_0^{\frac{p_0-1}{q_0}}$. Replacing $d(t)$ by its expression in (48) yields:

$$\begin{aligned} \dot{s}_1 &= \Delta f_3 - \lambda s_1 - \mu s_1^{\frac{v}{w}} \\ &\quad - \frac{\Delta g_3}{\hat{g}_3} \left[\hat{f}_3 + A + \lambda s_1 + \mu s_1^{\frac{v}{w}} \right] \end{aligned} \tag{49}$$

Then, we obtain

$$\begin{aligned} \dot{s}_1 &= \Delta f_3 - b\hat{f}_3 - bA - \lambda(b + 1)s_1 - \mu(b + 1)s_1^{\frac{v}{w}} \\ \dot{s}_1 &= -\lambda(b + 1)s_1 \\ &\quad - (\mu(b + 1) - \frac{\Delta f_3 - b\hat{f}_3 - bA}{s_1^{\frac{v}{w}}}) s_1^{\frac{v}{w}} \end{aligned} \tag{50}$$

$$\dot{s}_1 = -\lambda_1 s_1 - \mu_1 s_1^{\frac{v}{w}}$$

In order to fulfill fast terminal sliding mode convergence, the following inequalities must be satisfied:

$$\begin{aligned} \lambda_1 &= \lambda(b + 1) > 0 \\ \mu_1 &= \mu(b + 1) - \frac{\Delta f_3 - b\hat{f}_3 - bA}{s_1^{\frac{v}{w}}} > 0 \end{aligned} \tag{51}$$

As it has been introduced, $\lambda > 0, b = \frac{\Delta g_3}{\hat{g}_3}$ and $\frac{g_3}{\hat{g}_3} > 0$ then we have

$$b + 1 = \frac{\Delta g_3}{\hat{g}_3} + 1 = \frac{g_3 - \hat{g}_3}{\hat{g}_3} + 1 = \frac{g_3}{\hat{g}_3} > 0$$

Then the condition $\lambda_1 = \lambda(b + 1) > 0$ is satisfied.

According to (46), we obtain the following inequality:

$$\begin{aligned} \mu(b + 1) &- \frac{\Delta f_3 - b\hat{f}_3 - bA}{s_1^{\frac{v}{w}}} \\ &= \sigma + \frac{L}{|s_1|^{\frac{v}{w}}} - \frac{\Delta f_3 - b\hat{f}_3 - bA}{s_1^{\frac{v}{w}}} \end{aligned}$$

$$> \sigma + \frac{L}{|s_1|^{\frac{v}{w}}} - \frac{|\Delta f_3 - b\hat{f}_3 - bA|}{|s_1|^{\frac{v}{w}}} \geq \sigma > 0$$

It's obvious that in the following region Δ satisfying:

$$|s_1| > \left[\frac{L}{\mu(b+1)} \right]^{\frac{w}{v}}, \text{ the condition } \mu_1 > 0 \text{ is held.}$$

And then

$$\lambda_1 > 0$$

$$\mu_1 > 0$$

Considering the following Lyapunov function:

$$V_1 = \frac{1}{2} s_1^2 \tag{52}$$

Deriving V_1 yields:

$$\dot{V}_1 = s_1 \dot{s}_1 \tag{53}$$

$$\dot{V}_1 = s_1 (-\lambda_1 s_1 - \mu_1 s_1^{\frac{v}{w}}) = -\lambda_1 s_1^2 - \mu_1 s_1^{\frac{v}{w}+1}$$

$$\leq -\mu_1 2^{\frac{v+w}{2w}} V^{\frac{v+w}{2w}}$$

According to *Lemma 1*, the controlled system fulfills MPPT with robustness and will attain the region Δ at finite time.

4. Comparison with Conventional Methods of MPPT

In this section, a comparative study is presented between the proposed controller and two conventional MPPT methods. The chosen traditional techniques are PI and P&O controllers.

Equation (54) gives the PI controller expression [28]:

$$d(t) = K_p e_1(t) + K_i \int_0^t e_1 d\tau \tag{54}$$

Among the utilized MPPT techniques, the most preferred is the perturb and observe scheme. This algorithm is easy in practice and in implementation. Figure 6 clarifies its principle.

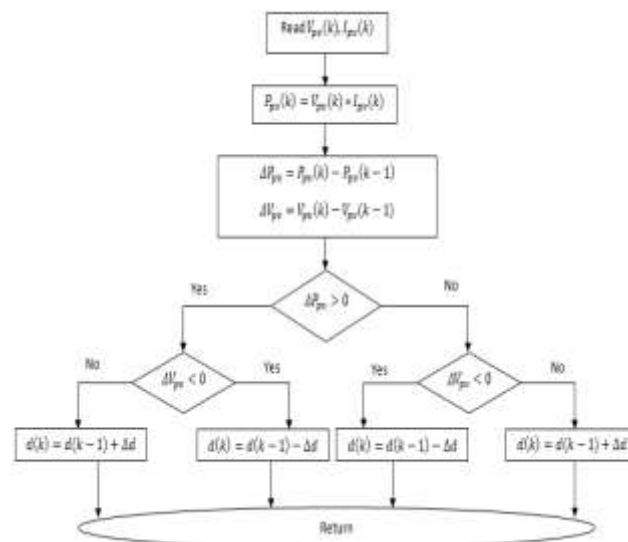


Fig.6. Law diagram of the P&O technique

5. Numerical Simulation Results

Validating the designed MPPT method requires a PV structure composed by a 200 W PV module KC200GH-2P and a boost converter. The used module characteristics are shown in table 1, the boost converter parameters are given below [24]:

$$L = 1.21 \text{ mH}, R_c = 36.9 \Omega, C_1 = C_2 = 1000 \mu\text{F},$$

$$R = 25 \Omega \text{ and } V_D = 0.82 \text{ V.}$$

Table 1. Parameters of the used photovoltaic module.

Maximum power P_{max}	200W ± 10%
Maximum current i_{max}	7.61 A
Open circuit voltage V_{oc}	32.9 V
Short circuit current i_{scr}	8.21 A
Short circuit current temperature coefficient K_I	$4.79 \times 10^{-3} \text{ A}/^\circ\text{C}$
Factor n	1.8

Moreover, the controller parameters are set as follows:

$$\alpha_0 = 1500,; \beta_0 = 10; \alpha_1 = 1000; \beta_1 = 10;$$

$$p_0 = 5; q_0 = 9; p_1 = 5; q_1 = 9;$$

Then, two simulation scenarios based on fixed irradiance and varying irradiance are conducted.

5.1. Fixed atmosphere conditions

As a first step, a fixed irradiance at $1000 \text{ W}/\text{m}^2$ and 25°C cell temperature are set. The MPPT scheme based on FTSMC is considered and simulation results are given in Figs.7-12. As shown in Figs.7-8, the reference voltage $V_{ref} = 26.3 \text{ V}$ and the maximum power 200 W are attained at $t = 0.006 \text{ s}$. This shows that the designed

control scheme fulfills the maximum power point tracking rapidly, accurately and offers high performances of robustness against parameter uncertainties. Meanwhile, the control signal does not present a phenomenon of chattering as in traditional sliding mode owing to the fact that errors reach zero in limited time.

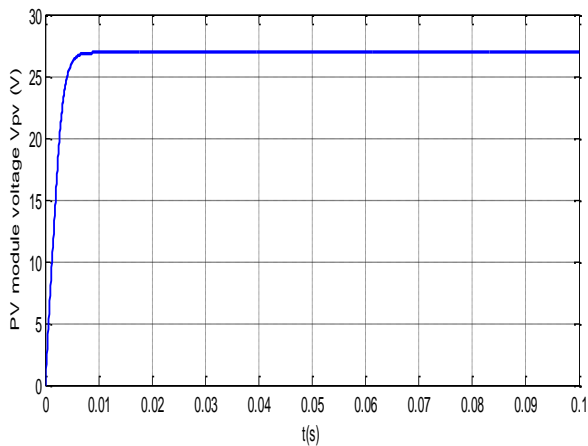


Fig.7. Behavior curve of PV module output voltage

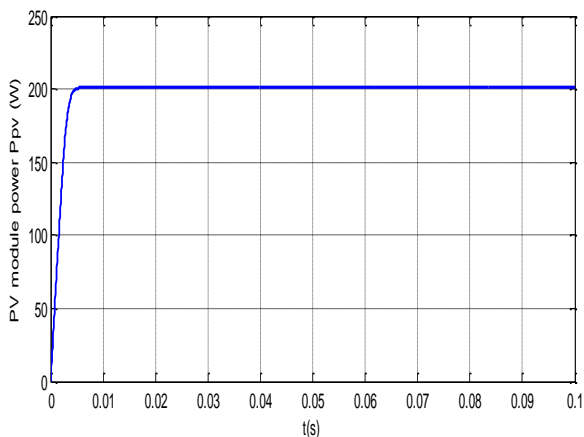


Fig.8. Behavior curve of PV module output power

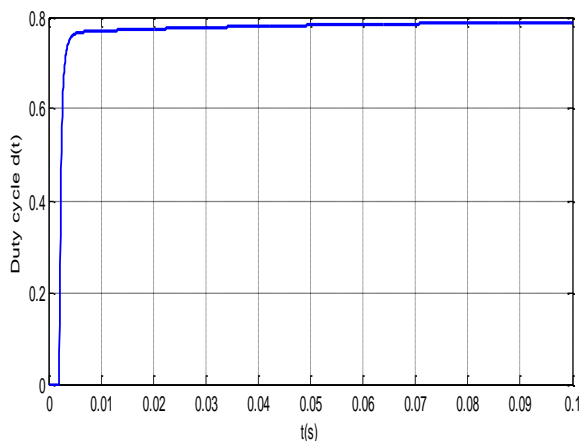


Fig.9. MPPT control response of the duty cycle $d(t)$

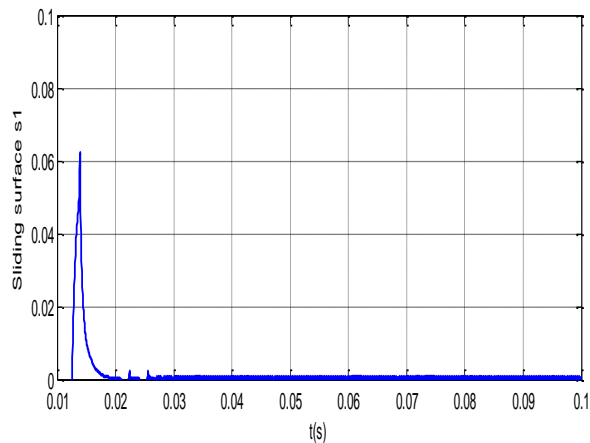


Fig.10. MPPT control response of the sliding surface $s_1(t)$

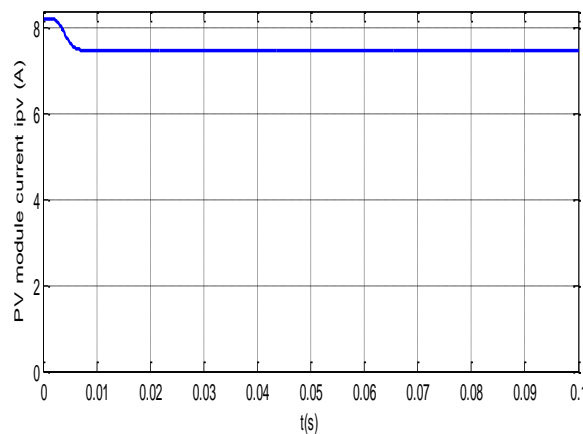


Fig.11. MPPT control behavior of PV module output current $I_{pv}(t)$

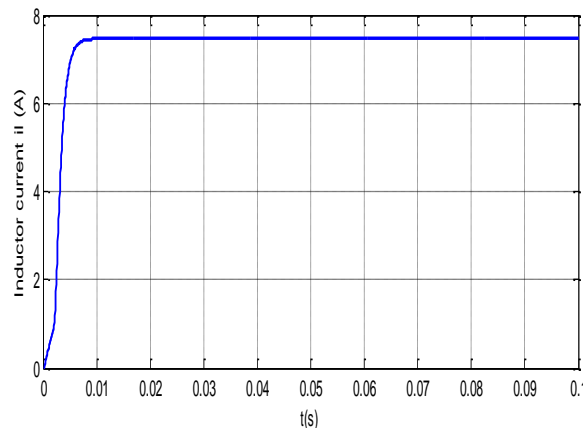


Fig.12. MPPT control behavior of inductor current $i_L(t)$

5.2. Varying atmosphere conditions

In this case, simulation have been conducted for initial conditions $E = 1000W/m^2$ and $T = 25^\circ C$ and then for successive radiation steps applied at $t=1s$ ($E = 200W/m^2$) and $t=2s$ ($E = 600W/m^2$). The same simulations

have been carried out for the PI controller and P&O controller in order to compare them with the proposed FTSM controller results. The PI control gains are chosen as follows: $K_p = 15$ and $K_i = 0.01$. Simulation results showing PV module power P_{pv} and output voltage V_{pv} have been compared respectively with the optimal power P_{op} and the optimal voltage V_{op} issued from the MPP searching algorithm.

It can be seen from Figs.13-16 that the FTSM controller exhibits much lower chattering phenomenon and a faster response compared with the PI controller and P&O controller. Furthermore, PI controller has a lower power output and a higher output voltage compared with the FTSM controller at the first irradiance step.

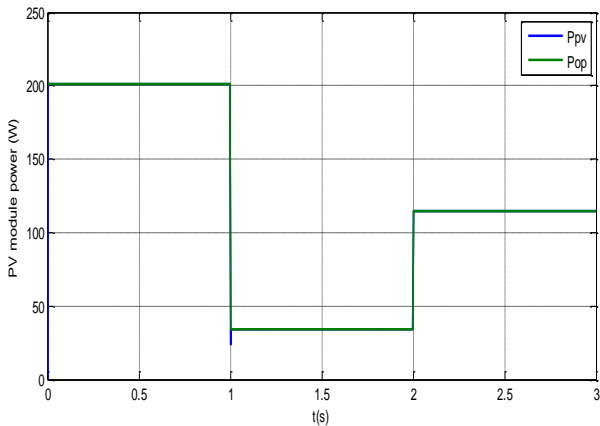


Fig.13. PV module power behavior with FTSMC

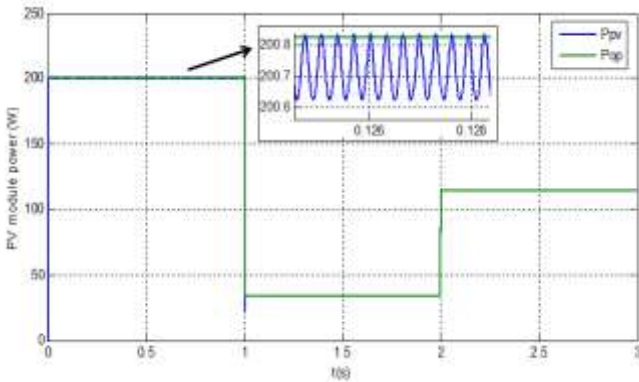


Fig.14. PV module power behavior with PI controller

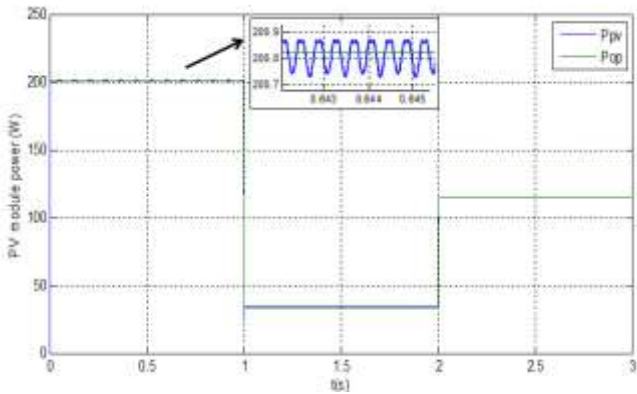


Fig.15. PV module power behavior with P&O controller

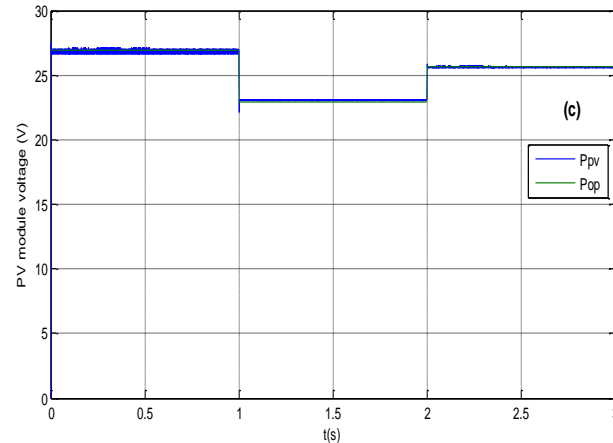
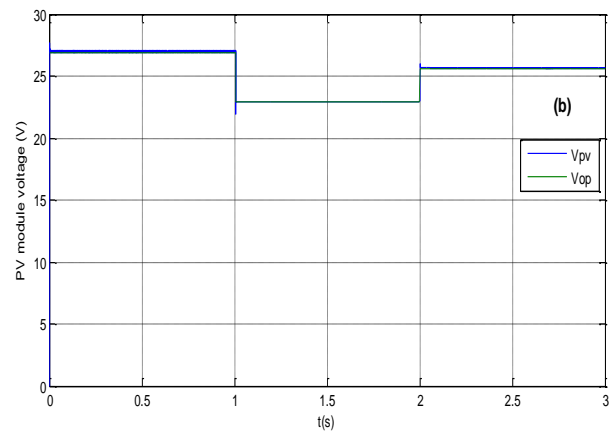
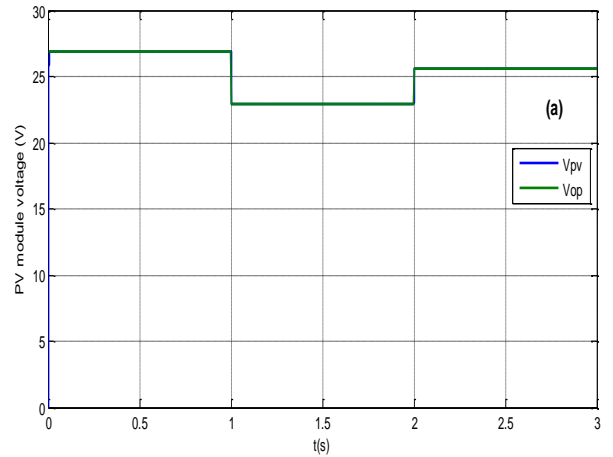


Fig.16. PV module output voltage behavior with (a) FTSMC (b) PI controller (c) P&O controller

Then a fixed temperature $T = 25^{\circ}\text{C}$ and a sinusoidal varying radiation E are applied to the control scheme. E is given as follows:

$$E = 1000 \sin\left(\frac{\pi}{12}(t - 6)\right)$$

The behavior of the irradiance is given in Fig.17.

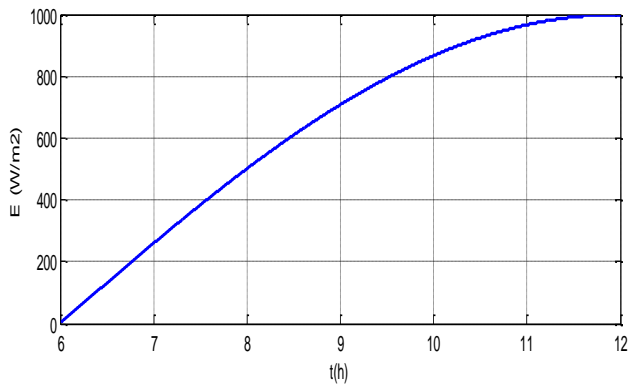


Fig.17. Irradiance profile

The same atmosphere conditions have been applied to the PI and P&O controllers. The $(P_{pv} - V_{pv})$ characteristics given in Fig.18 show that the designed MPPT control scheme has a smoother response and presents no chattering phenomenon. Meanwhile, the conventional controllers used exhibit an oscillating response which means that a part of the usable power issued from the photovoltaic model is wasted and therefore, efficiency of the whole generation system is decreased.

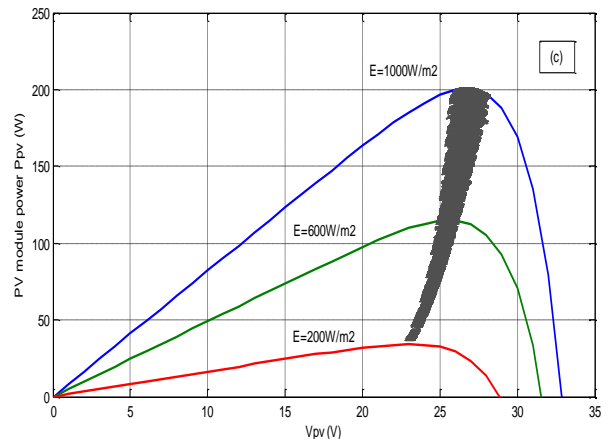
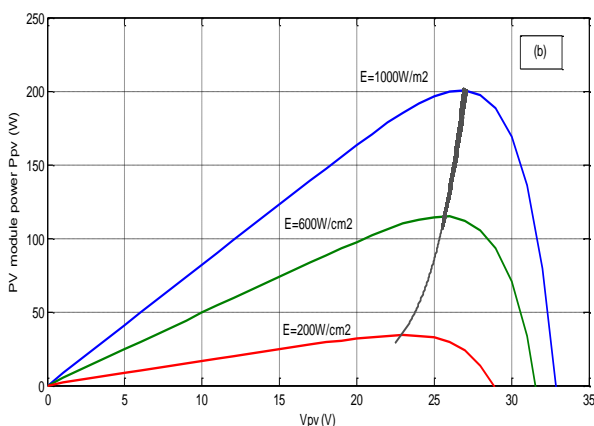
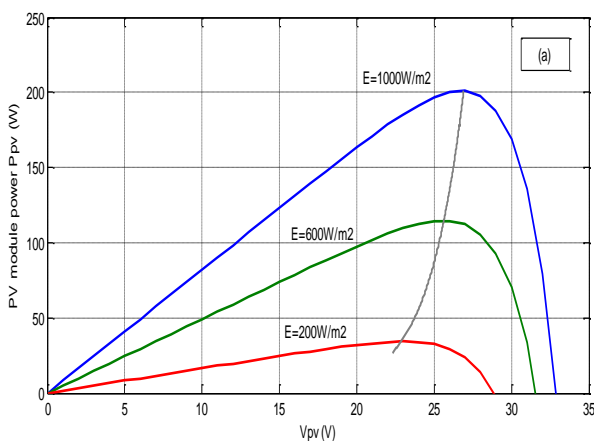


Fig.18. $(P_{pv} - V_{pv})$ characteristic behavior undersinusoidal irradiance with (a) FTSMC (b) PI controller (c) P&O controller at 25°C



6. Conclusions

During this work, the FTSMC is utilized for MPPT in standalone photovoltaic structures. Even in presence of parameter uncertainties, the proposed control scheme provides convergence in limited time. By using the FTSMC controller and the proposed searching algorithm, the MPPT is fulfilled even in transient change of atmosphere conditions.

Moreover, simulations have shown that the designed MPPT control performances are better than those obtained from traditional MPPT techniques. The simulation results issued from traditional algorithms are subject of chattering phenomenon, imprecise and slow response. As matter of fact, the FTSMC controller utilized in this paper offers high robustness towards uncertainties, accurate and rapid response to changing atmosphere and enhanced tracking performances.

References

- [1] J. Ahmed and Z. Salam, "An improved perturb and observe (P&O) maximum power point tracking (MPPT) algorithm for higher efficiency", *Applied Energy*, vol. 150, pp. 97–100, 2015.
- [2] B. Bendib, H. Belmili and F. Krim, "A survey of the most used MPPT methods: Conventional and advanced algorithms applied for photovoltaic systems", *Renewable and Sustainable Energy Reviews*, vol. 45, pp. 637–648, 2015.
- [3] A. Harrag and S. Messalti, "Variable step size modified P&O MPPT algorithm using GA-based hybrid offline/online PID controller", *Renewable and Sustainable Energy Reviews*, vol. 49, pp. 247–260, 2015.
- [4] K. Soon Tey and S. Mekhilef, "Modified incremental conductance MPPT algorithm to mitigate inaccurate

- responses under fast-changing solar irradiation level”, *Solar Energy*, vol.101, pp.333–342, 2014.
- [5] A. Loukriz, M. Haddadi and S. Messalti, “Simulation and experimental design of a new advanced variable step size Incremental Conductance MPPT algorithm for PV systems”, *ISA Transactions*, vol.62, pp.30–38, 2016.
- [6] H. Boumaaraf, A. Talha and O. Bouhali, “A three-phase NPC grid-connected inverter for photovoltaic applications using neural network MPPT”, *Renewable and Sustainable Energy Reviews*, vol.49, pp.1171–1179, 2015.
- [7] H. Rezk and E. Hasaneen, “A new MATLAB/Simulink model of triple-junction solar cell and MPPT based on artificial neural networks for photovoltaic energy systems”, *Ain Shams Engineering Journal*, vol.6, pp. 873–881, 2015.
- [8] Y-T.Chen, Y-C. Jhang and R-H. Liang, “Fuzzy-logic based auto-scaling variable step-size MPPT method for PV systems”, *Solar Energy*, vol.126, pp.53–63, 2016.
- [9] B. Bendiba, F. Krimb, H. Belmilia, M. F. Almia and S. Bouloumaa “Advanced Fuzzy MPPT Controller for a stand-alone PV system”, *Energy Procedia*, vol.50, pp. 383 – 392, 2014.
- [10] I.S. Kim, “Robust maximum power point tracker using sliding mode controller for the three phase grid-connected photovoltaic system”, *Solar Energy*, vol.84, no.12, pp.2219–2229, 2007.
- [11] M. Farhat, O. Barambones, and L. Sbita, “A new maximum power point method based on a sliding mode approach for solar energy harvesting”, *Applied energy*, In Press, Corrected Proof, 2016.
- [12] F.Zhang, J. Maddy, G. Premier and A. Guwy (2015), “Novel current sensing photovoltaic maximum power point tracking based on sliding mode control strategy” *Solar Energy*, vol.118, pp.80–86, 2015.
- [13] I.S. Kim, “Robust maximum power point tracker using sliding mode controller for the three-phase grid-connected photovoltaic system”, *Solar Energy*, vol.81, pp.405–414, 2007.
- [14] E. Bianconi, J. Calvente, R. Giral, E. Mamarelis, G. Petrone, C.A. Ramos-Paja, G. Spagnuolo and M. Vitelli, “A fast current-based MPPT technique employing sliding mode control”, *IEEE T. Ind. Electron.*, vol.60, no.3, pp.1168–1178, 2013.
- [15] D. Zhao, Q. Zhua and J. Dubeldamc, “Terminal sliding mode control for continuous stirred tank reactor”, *Chemical engineering research and design*, vol.94, pp. 266–274, 2015.
- [16] S-E. Li, K. Dung, K. Li and C. Ahn, (2015), “Terminal sliding mode control of automated car-following system without reliance on longitudinal acceleration information”, *Mechatronics*, vol. 30, pp.327–337, 2015.
- [17] X. Yu, and Z. Man, “Model Reference Adaptive Control Systems with Terminal Sliding Modes”, *International Journal of Control*, vol.64, pp.1165–1176, 1996.
- [18] Z. Man, and X. Yu, “Terminal Sliding Mode Control of MIMO Linear Systems”, *IEEE Transactions on Circuits and Systems I: Fundamental Theory and Applications*, vol. 44, pp.1065–1070, 1997.
- [19] Y. Wu, X. Yu, and Z. Man, “Terminal Sliding Mode Control Design for Uncertain Dynamic Systems”, *Systems and Control Letters*, vol.34, pp.281–288, 1998.
- [20] X. Yu, and Z. Man, “Fast Terminal Sliding-mode Control Design for Nonlinear Dynamical Systems”, *IEEE Transactions on Circuits and Systems I: Fundamental Theory and Applications*, vol. 49, pp. 261–264, 2002.
- [21] T. Madani, B. Daachi and K. Djouani, “Non-singular terminal sliding mode controller: Application to an actuated exoskeleton”, *Mechatronics*, vol.33, pp. 136–145, 2016.
- [22] A. Rezoug, B. Tondou, and M. Hamerlain, “Experimental Study of Nonsingular Terminal Sliding Mode Controller for Robot Arm Actuated by Pneumatic Artificial Muscles”, *The International Federation of Automatic Control Cape Town, South Africa’2014*, pp. 10113–10118, 2014.
- [23] H-H. Doostabad, R. Keypour, M-R. Khalghani and M-H. Khooban, “A new approach in MPPT for photovoltaic array based on Extremum Seeking Control under uniform and non-uniform irradiances”, *Solar Energy*, vol. 94, pp.28–36, 2013.
- [24] C-S. Chui, Y-L. Ouyang, and C-Y. Ku, “Terminal sliding mode control for maximum power point tracking of photovoltaic power generation systems” *Solar Energy*, vol. 86, pp.2986–2995, 2012.
- [25] M-F. Mimouni, M-N. Mansouri, B. Benhanem and M. Annabi, “Vectorial command of an asynchronous motor fed by a photovoltaic generator”, *Renewable Energy*, vol. 29, pp. 433–442, 2004.
- [26] Y. Feng, X. Yu, and Z. Man, “Non-singular terminal sliding mode control of rigid manipulators”, *Automatica*, vol.38, no.12, pp. 2159–2167, 2002.
- [27] Y. Feng, L-X. Sun and X-H. Yu, (2004), “Finite time synchronization of chaotic with unmatched uncertainties,” 30th Annual Conference of the IEEE Industrial Electronics Society, pp.2911–6, 2004.
- [28] E. Koutroulis, K. Kalaitzakis, N.C. Voulgaris, “Development of a microcontroller-based, photovoltaic maximum power point tracking control system”, *IEEE Transactions on Power Electronics*, vol.16, no.1, pp.46–54, 2001.